



Hirshfeld surface analysis, FTIR and UV-Visible spectroscopic and DFT investigations of p-Carboxyphenylammonium dihydrogenmonophosphate monohydrate

Abdellatif Rafik^{1*}, Hafid Zouihri², Taoufiq Guedira¹

¹Laboratory of Materials, Electrochemistry and Environment Faculty of Sciences, Chemistry department, Ibn Tofail University Kenitra, Morocco .

²Laboratory of Materials Chemistry and Biotechnology of Natural Products, Moulay Ismail University, Faculty of Sciences, Meknes, Morocco.

Received 14 May 2019,
Revised 18 Dec 2019,
Accepted 23 Dec 2019

Keywords

- ✓ Organic–inorganic hybrid material,
- ✓ Single crystal X-ray diffraction,
- ✓ 3-D Hirshfeld surface,
- ✓ Intermolecular Interactions,

abdellatif.rafik@uit.ac.ma
Phone: +212644435253;

Abstract

Single crystals of the title organic–inorganic hybrid compound have been grown by slow evaporation solution growth technique at 50°C. The grown crystals were subjected to various studies such as single crystal X-ray diffraction (XRD),MEB-EDAX, UV-Vis studies, Fourier Transform Infrared (FTIR).The title compound crystallizes in the triclinic crystal system with the space group P-1 and the lattice parameters $a(\text{Å}) = 8.5304(5)$, $b(\text{Å}) = 8.9095(5)$, $c(\text{Å}) = 14.4986(2)$, $\alpha(^{\circ}) = 106.413(2)$, $\beta(^{\circ}) = 90.158$, $\gamma(^{\circ}) = 92.830(3)$ and $V(\text{Å}^3) = 1055.56(10)$. The Hirshfeld surface and the associated 2D fingerprint plots were investigated which revealed that more than two-third of close contacts were associated with relatively weak $\text{H}\cdots\text{H}$, $\text{O}\cdots\text{H}$ and $\text{O}\cdots\text{C}$ interactions.

1. Introduction

The synthesis of hybrid phosphates involves both organic and inorganic components blended in the solid state on the molecular scale. Such materials allow the combination of the intended properties of both the organic and inorganic components when they self-assemble in the crystal. The resulting properties do not simply consist of the sum of the individual contributions, since they also strongly depend on the nature of the interactions established by the different components within the structure. The nature of the interactions has been used to divide organic–inorganic hybrid materials into two different classes, both of them being of technological interest. In class I, organic and inorganic components are connected together through strong chemical covalent or ionic-covalent bonds; in class II, the two components are assembled by weaker interactions, such as hydrogen bonds and/or van der Waals and Coulombic interactions.

In particular, in considering hybrid systems belonging to class II, derivatives from orthophosphoric acid (H_3PO_4) are often associated with functionalized organic molecules (amines or amides) to produce organic–inorganic materials with potentially forceful hydrogen-bonding interactions between donor (D) and acceptor (A) components. Among these hybrid phosphates, the dihydrogen phosphates have received great interest over recent years. Indeed, these compounds can be considered the most stable organic phosphates and also the first to be studied in more detail.

As the presence of water in the structures of protonconducting salts usually undesirably decreases their chemical stability and makes them unsuitable for applications at elevated temperatures [1]. Organic monohydrogen (HPO_4)²⁻ and dihydrogen phosphate (H_2PO_4)⁻ compounds provide a class of

materials with numerous practical and potential uses in various fields such as biomolecular sciences, catalysis, ferroelectrics, non-linear optical and supramolecular studies [2-4].

Recently a series of compounds based on hydrogen and dihydrogen monophosphate cluster (HPO_4^{2-}) and (H_2PO_4^-) linked through organoamine bases has been reported, such as $[\text{C}_{11}\text{H}_{17}\text{N}_4^+][(\text{H}_2\text{PO}_4^-)]$ [5], $[\text{C}_6\text{H}_8\text{NO}^+][(\text{H}_2\text{PO}_4^-)]$ [6], $[\text{C}_6\text{H}_6\text{NO}_2^+][(\text{H}_2\text{PO}_4^-)]$ [7], $[\text{C}_9\text{NH}_8^+][(\text{H}_2\text{PO}_4^-)]$ [8], $[\text{C}_6\text{H}_{10}\text{N}_3\text{O}_2^+][\text{H}_3\text{PO}_4][\text{H}_2\text{PO}_4^-]$ [9], $[\text{C}_7\text{H}_7\text{N}_2\text{S}^+][\text{H}_2\text{PO}_4^-]$ [10], $[\text{C}_{12}\text{H}_{17}\text{N}_2\text{S}^+][\text{H}_2\text{PO}_4^-]$ [11], $[\text{C}_6\text{H}_{21}\text{N}_4^{3+}][\text{HPO}_4^{2-}][\text{H}_2\text{PO}_4^-]$ [12], $[\text{C}_6\text{H}_9\text{N}_2\text{O}_2\text{S}^+][\text{H}_2\text{PO}_4^-]$ [13], $[\text{C}_6\text{H}_8\text{N}^+][\text{H}_2\text{PO}_4^-]$ [14], $[\text{C}_5\text{H}_6\text{N}_5^+][\text{H}_2\text{PO}_4^-]$ [15], $[\text{C}_{13}\text{H}_{12}\text{N}_3^+][\text{H}_2\text{PO}_4^-]$ [16], $[(\text{C}_4\text{H}_6\text{N}_3^+)][(\text{H}_2\text{PO}_4^-)].\text{H}_2\text{O}$ [17].

Using the theoretical calculations applied to the hybrid, we can get an idea about interactions, energy, optic nonlinear properties and other characteristics of their structures.

In the majority of previous works, such theoretical studies were not systematically performed on di-hydrogen monophosphate. That is, a large number of Strandberg structures were synthesized and characterized but not theoretically studied. Herein, we focus on the semiempirical calculations employed to investigate this type of compounds. In this paper, we report the synthesis and crystal structure of a new title compound PABADHP, study its non-bonding interactions with the help of Hirshfeld surfaces, and discuss the results of theoretical calculations.

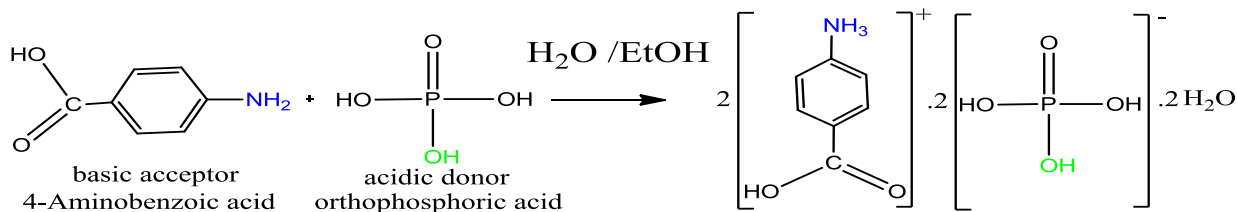
2. Experimental and theoretical

2.1. Materials and measurements

For the title compound, all reagents were purchased commercially and used without further purification. 4-Aminobenzoic acid (purity 99 %,.) and orthophosphoric acid (85%wt, $d = 1.7 \text{ kg.cm}^{-3}$) were from Sigma–Aldrich. The infrared spectrum of PABADHP was recorded at room temperature on a Perkin-Elmer Spectrometer (ATR-FTIR) between 4000 and 500 cm^{-1} . A Perkin-Elmer Lambda-19 spectrophotometer was used to measure UV–Vis spectra in the 190–600 nm range using aqueous solutions. The energy dispersive analysis was performed using the Electron microscope Smart Quant model coupled to an X-ray energy dispersion analysis spectrometer.

2.2. Synthesis

The synthesis of p-Carboxyphenylammonium dihydrogenmonophosphate monohydrate crystals were grown by the slow evaporation solution growth technique. The supersaturated solution maintained at 50°C of was prepared by mixing equal proportion of p-Carboxyphenylammonium (purity 99 %,.) and orthophosphoric acid (85%wt, $d = 1.7 \text{ kg cm}^{-3}$) in 10 ml of a mixture of water and ethanol (50%-50%) (Fig.1). The growth solution was maintained at constant temperature (45°C) to attain equilibrium state and excess amount of solvent has been evaporated, after three days. After a small speck of crystal was observed (Fig.2 and 3), the temperature was decreased by 5°C per day as the growth progressed. Single crystals of the title compound, suitable for X-ray diffraction analysis, were obtained after one week (yield 88%). An EDAX spectrum confirming the presence of C, N, O, and P is shown in Fig. 4.



p-Carboxy phenylammonium dihydrogenmonophosphate monohydrate

Figure1. Schematic drawing of the formation of PABADHP.

2.3. X-Ray Crystal Structures

The crystal structure was determined from the single-crystal X-ray diffraction data collected at room temperature using a Bruker AXS CCD area detector system equipped with graphite monochromatic $\text{MoK}\alpha$ radiation (0.71073 Å). The Phosphorus atom was located using the Patterson methods with program SHELXS-86 [18].



Figure 2. Photograph of a grown crystal of PABADHP.

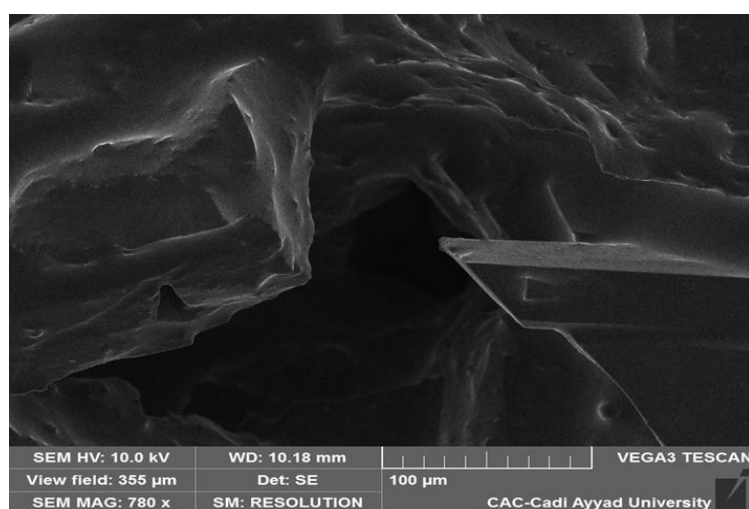


Figure 3. Surface micrograph of PABADHP.

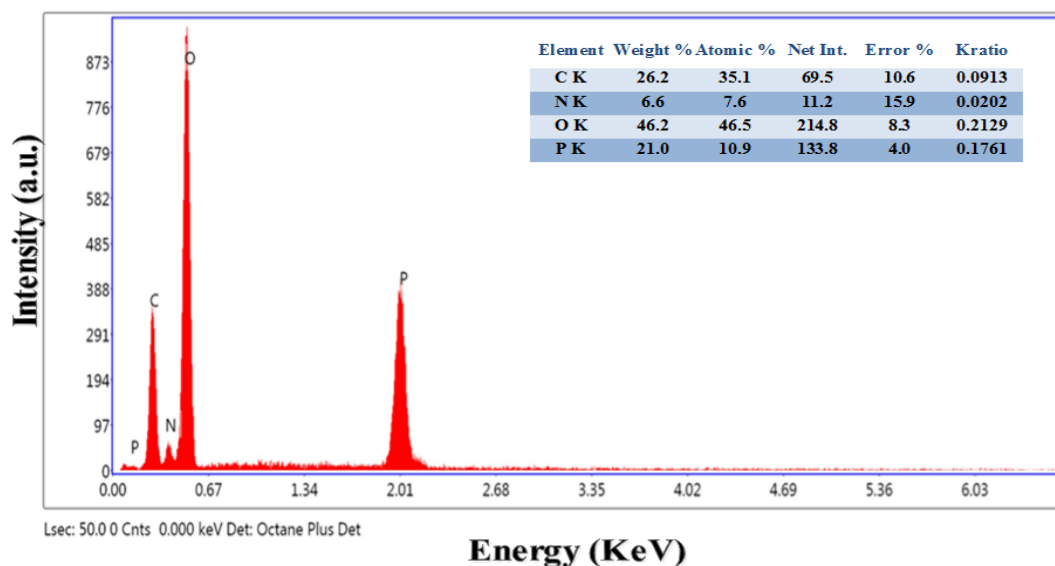


Figure 4. The EDAX Spectrum of PABADHP, showing the presence of C, N, O, and P.

The oxygen atoms of water and the organic moieties were found from successive Fourier calculations using SHELXL-97[19]. All the hydrogen atoms were placed geometrically and refined isotropically. The H atoms were located in a difference Fourier map and refined as riding, with O—H = 0.82 Å, N—H = 0.89 Å, C—H = 0.93 and 0.97 Å. The dihydrogen phosphate H atoms were refined with $U_{iso}(H) = 1.5U_{eq}(O)$, those of the ammonium H atoms with $U_{iso}(H) = 1.5U_{eq}(N)$, and the remaining ones with $U_{iso}(H) = 1.2U_{eq}(C)$.

The pertinent experimental details of the structure determination for the new compound are presented in Table 1. The refinement was done by full-matrix least squares methods (SHELXL-97 program) and converged to an acceptable final agreement factor. The last cycle of refinement included the atomic coordinates for all the atoms, anisotropic thermal and isotropic thermal parameters, Atomic displacement parameters (\AA^2), Geometric parameters ($\text{\AA},^\circ$) and Hydrogen-bond geometry ($\text{\AA},^\circ$). Whose values are listed in Table 2, 3 and 4 respectively. The structural graphics of the asymmetric unit and the crystal packing were created with PLATON [20] and DIAMOND programs [21].

Table 1. Experimental data for PABADHP

Crystal data	
Chemical formula	$\text{C}_7\text{H}_8\text{O}_2\text{N}^+\cdot\text{H}_2\text{PO}_4^-\cdot\text{H}_2\text{O}$
Formula weight (g mol^{-1})	253.15
D_x (Mg m^{-3})	1.593
Temperature (K)	296
Wavelength (\AA)	Mo $K\alpha$ radiation, $\lambda = 0.71073 \text{\AA}$
Crystal system, space group	Triclinic, $P-1$
a, b, c (\AA)	8.5304 (5), 8.9095 (5), 14.4986 (8)
α, β, γ ($^\circ$)	106.413 (2), 90.158 (2), 92.830 (3)
Cell volume (\AA^3)	1055.56 (10)
Z	4
μ (mm^{-1})	0.28
Goodness-of-fit	1.06
Weighting scheme	$w = 1/[\sigma^2(F_o^2) + (0.0545P)^2 + 0.2536P]$ where $P = (F_o^2 + 2F_c^2)/3$
Final indices $R[F^2 > 2\sigma(F^2)], wR(F^2)$,	$R1 = 0.031, wR2 = 0.093$
R indices (all data)	$R1 = 0.017, wR2 = 0.093$
Measured reflections	15888
Independent reflections	4594
Data/restraints/parameters	4594 /12/354
$(\sin \theta/\lambda)_{\max}$ (\AA^{-1})	0.639
$R[F^2 > 2\sigma(F^2)], wR(F^2), S$	0.031, 0.093, 1.06
$\theta_{\max}, \theta_{\min}$ ($^\circ$)	27.0, 2.4
h, k, l	(-10 \rightarrow 10), (-11 \rightarrow 11), (-18 \rightarrow 17)
$\Delta)_{\max}, \Delta)_{\min}$ ($e \text{\AA}^{-3}$)	0.30, -0.33

Table 2. Fractional atomic coordinates and isotropic or equivalent isotropic displacement parameters (\AA^2)

	x	y	z	$U_{\text{iso}}^*/U_{\text{eq}}$
H12O	0.210 (3)	0.375 (3)	-0.1849 (19)	0.079 (8)*
H13O	0.296 (3)	0.841 (3)	-0.175 (2)	0.081 (8)*
P1	0.82743 (4)	0.27859 (4)	0.36321 (2)	0.02571 (11)
O1	0.88687 (12)	0.16158 (12)	0.41089 (7)	0.0303 (2)
O4	0.68932 (12)	0.22033 (14)	0.29544 (7)	0.0340 (2)
O2	0.78267 (15)	0.42404 (14)	0.44690 (7)	0.0389 (3)
O3	0.96783 (14)	0.33467 (15)	0.30939 (8)	0.0398 (3)
O9	0.40270 (13)	0.25998 (13)	0.39023 (7)	0.0331 (2)
P2	0.67376 (4)	0.76679 (4)	0.36589 (2)	0.02656 (11)
O5	0.60500 (12)	0.65047 (12)	0.41458 (7)	0.0311 (2)
O7	0.80935 (12)	0.71045 (14)	0.30122 (7)	0.0359 (3)
O6	0.72577 (15)	0.91710 (14)	0.44875 (7)	0.0390 (3)
O8	0.53893 (14)	0.81464 (15)	0.30748 (8)	0.0401 (3)
O10	0.09368 (13)	0.75448 (13)	0.39392 (7)	0.0317 (2)
O12	0.21071 (14)	0.42044 (15)	-0.11855 (8)	0.0403 (3)
O13	0.30081 (13)	0.88347 (16)	-0.11209 (8)	0.0414 (3)
O14	0.06533 (15)	0.75887 (15)	-0.12073 (7)	0.0441 (3)
O11	0.40549 (16)	0.26105 (16)	-0.12154 (8)	0.0489 (3)
C3	0.31124 (17)	0.48539 (16)	0.22733 (9)	0.0259 (3)
C6	0.31362 (17)	0.40701 (16)	0.02963 (9)	0.0280 (3)

C7	0.31501 (18)	0.35622 (17)	-0.07753 (10)	0.0303 (3)
C5	0.19908 (19)	0.49999 (19)	0.07959 (10)	0.0343 (3)
H5	0.1232	0.5367	0.0464	0.041*
C4	0.19718 (18)	0.53868 (19)	0.17931 (10)	0.0336 (3)
H4	0.1195	0.6000	0.2132	0.040*
C1	0.4287 (2)	0.3558 (2)	0.07972 (10)	0.0371 (4)
H1	0.5063	0.2939	0.0461	0.045*
C2	0.4292 (2)	0.3959 (2)	0.17928 (10)	0.0371 (4)
H2	0.5074	0.3632	0.2130	0.045*
C14	0.17548 (17)	0.83729 (17)	-0.07426 (10)	0.0288 (3)
C10	0.16872 (17)	0.97866 (16)	0.23095 (9)	0.0258 (3)
C13	0.17512 (17)	0.88953 (16)	0.03302 (10)	0.0278 (3)
C11	0.03234 (18)	0.91597 (18)	0.17929 (10)	0.0325 (3)
H11	-0.0604	0.9048	0.2108	0.039*
C9	0.30701 (18)	0.99725 (19)	0.18590 (10)	0.0344 (3)
H9	0.3975	1.0389	0.2218	0.041*
C8	0.30969 (18)	0.9532 (2)	0.08653 (10)	0.0348 (3)
H8	0.4023	0.9664	0.0554	0.042*
C12	0.03688 (18)	0.87038 (18)	0.07992 (10)	0.0320 (3)
H12	-0.0532	0.8266	0.0442	0.038*
N2	0.16621 (16)	1.02462 (15)	0.33631 (8)	0.0286 (3)
N1	0.30990 (16)	0.52465 (15)	0.33269 (8)	0.0286 (3)
H3O	0.953 (3)	0.302 (3)	0.2490 (19)	0.076 (8)*
H6O	0.772 (3)	0.986 (3)	0.4303 (15)	0.052 (6)*
H12N	0.229 (2)	0.589 (2)	0.3527 (14)	0.050 (6)*
H11N	0.305 (2)	0.437 (2)	0.3489 (15)	0.056 (6)*
H10N	0.401 (2)	0.575 (2)	0.3580 (14)	0.050 (6)*
H20N	0.253 (2)	1.087 (2)	0.3588 (14)	0.049 (5)*
H21N	0.162 (2)	0.939 (2)	0.3559 (14)	0.047 (5)*
H22N	0.0794 (19)	1.078 (2)	0.3576 (13)	0.038 (5)*
H9B	0.410 (3)	0.284 (3)	0.4529 (12)	0.071 (7)*
H9A	0.4976 (19)	0.245 (2)	0.3633 (14)	0.052 (6)*
H10B	-0.0006 (19)	0.736 (2)	0.3668 (13)	0.046 (5)*
H10A	0.091 (2)	0.771 (2)	0.4564 (11)	0.049 (5)*
H2O	0.728 (3)	0.489 (3)	0.4294 (17)	0.065 (7)*
H8O	0.561 (3)	0.791 (3)	0.2495 (19)	0.076 (8)*

Table 3. Atomic displacement parameters (\AA^2)

	U^{11}	U^{22}	U^{33}	U^{12}	U^{13}	U^{23}
P1	0.0296 (2)	0.0308 (2)	0.01655 (17)	0.00310 (14)	0.00060 (13)	0.00628 (13)
O1	0.0358 (6)	0.0323 (5)	0.0236 (5)	0.0057 (4)	0.0003 (4)	0.0084 (4)
O4	0.0289 (5)	0.0521 (7)	0.0194 (5)	0.0018 (5)	0.0002 (4)	0.0075 (4)
O2	0.0553 (7)	0.0372 (6)	0.0231 (5)	0.0156 (5)	-0.0006 (5)	0.0045 (4)
O3	0.0406 (6)	0.0540 (7)	0.0243 (5)	-0.0118 (5)	-0.0007 (5)	0.0128 (5)
O9	0.0331 (6)	0.0440 (6)	0.0210 (5)	0.0004 (5)	0.0015 (4)	0.0079 (4)
P2	0.0306 (2)	0.0320 (2)	0.01677 (17)	-0.00113 (14)	-0.00051 (13)	0.00694 (14)
O5	0.0372 (6)	0.0326 (5)	0.0234 (5)	-0.0029 (4)	0.0003 (4)	0.0087 (4)
O7	0.0314 (5)	0.0559 (7)	0.0196 (5)	0.0015 (5)	-0.0007 (4)	0.0093 (5)
O6	0.0554 (7)	0.0354 (6)	0.0232 (5)	-0.0123 (5)	-0.0012 (5)	0.0059 (4)
O8	0.0426 (6)	0.0558 (7)	0.0238 (5)	0.0130 (5)	0.0000 (5)	0.0126 (5)
O10	0.0317 (6)	0.0428 (6)	0.0199 (5)	0.0035 (4)	-0.0008 (4)	0.0073 (4)
O12	0.0422 (6)	0.0568 (7)	0.0211 (5)	0.0127 (5)	-0.0037 (4)	0.0079 (5)
O13	0.0356 (6)	0.0651 (8)	0.0201 (5)	-0.0032 (5)	0.0034 (4)	0.0074 (5)
O14	0.0508 (7)	0.0554 (7)	0.0217 (5)	-0.0149 (6)	-0.0012 (5)	0.0066 (5)
O11	0.0665 (8)	0.0592 (8)	0.0219 (5)	0.0282 (7)	0.0036 (5)	0.0086 (5)
C3	0.0305 (7)	0.0281 (7)	0.0179 (6)	-0.0033 (5)	-0.0009 (5)	0.0055 (5)
C6	0.0330 (7)	0.0304 (7)	0.0199 (6)	-0.0006 (6)	-0.0009 (5)	0.0064 (5)
C7	0.0355 (8)	0.0340 (7)	0.0211 (6)	0.0011 (6)	-0.0009 (6)	0.0073 (6)

C5	0.0344 (8)	0.0425 (8)	0.0244 (7)	0.0071 (6)	-0.0060 (6)	0.0062 (6)
C4	0.0329 (8)	0.0413 (8)	0.0236 (7)	0.0093 (6)	-0.0003 (6)	0.0033 (6)
C1	0.0431 (9)	0.0448 (9)	0.0240 (7)	0.0171 (7)	0.0036 (6)	0.0079 (6)
C2	0.0427 (9)	0.0475 (9)	0.0236 (7)	0.0169 (7)	-0.0005 (6)	0.0118 (6)
C14	0.0348 (8)	0.0315 (7)	0.0203 (6)	0.0044 (6)	0.0015 (5)	0.0072 (5)
C10	0.0331 (7)	0.0267 (6)	0.0176 (6)	0.0049 (5)	0.0015 (5)	0.0059 (5)
C13	0.0345 (7)	0.0289 (7)	0.0199 (6)	0.0036 (6)	0.0017 (5)	0.0065 (5)
C11	0.0313 (7)	0.0414 (8)	0.0243 (7)	-0.0046 (6)	0.0035 (6)	0.0097 (6)
C9	0.0291 (7)	0.0457 (9)	0.0239 (7)	0.0000 (6)	0.0001 (6)	0.0027 (6)
C8	0.0297 (7)	0.0483 (9)	0.0231 (7)	0.0004 (6)	0.0056 (6)	0.0049 (6)
C12	0.0323 (7)	0.0384 (8)	0.0240 (7)	-0.0043 (6)	-0.0014 (6)	0.0078 (6)
N2	0.0338 (7)	0.0337 (7)	0.0178 (5)	0.0031 (5)	0.0020 (5)	0.0061 (5)
N1	0.0336 (7)	0.0327 (6)	0.0185 (6)	0.0006 (5)	-0.0006 (5)	0.0060 (5)

Table 4. Geometric parameters (Å, °).

P1—O4	1.5059 (11)	C6—C1	1.388 (2)
P1—O1	1.5097 (10)	C6—C7	1.4907 (18)
P1—O3	1.5682 (11)	C5—C4	1.389 (2)
P1—O2	1.5685 (11)	C5—H5	0.9300
O2—H2O	0.85 (2)	C4—H4	0.9300
O3—H3O	0.85 (3)	C1—C2	1.386 (2)
O9—H9B	0.874 (16)	C1—H1	0.9300
O9—H9A	0.899 (15)	C2—H2	0.9300
P2—O7	1.5054 (11)	C14—C13	1.4924 (18)
P2—O5	1.5073 (10)	C10—C9	1.375 (2)
P2—O6	1.5694 (11)	C10—C11	1.386 (2)
P2—O8	1.5712 (12)	C10—N2	1.4659 (17)
O6—H6O	0.82 (2)	C13—C8	1.387 (2)
O8—H8O	0.83 (3)	C13—C12	1.390 (2)
O10—H10B	0.881 (15)	C11—C12	1.3831 (19)
O10—H10A	0.877 (15)	C11—H11	0.9300
O12—C7	1.3086 (18)	C9—C8	1.383 (2)
O12—H12O	0.93 (3)	C9—H9	0.9300
O13—C14	1.3040 (18)	C8—H8	0.9300
O13—H13O	0.89 (3)	C12—H12	0.9300
O14—C14	1.2209 (19)	N2—H20N	0.900 (15)
O11—C7	1.2180 (18)	N2—H21N	0.887 (15)
C3—C4	1.373 (2)	N2—H22N	0.906 (14)
C3—C2	1.380 (2)	N1—H12N	0.914 (15)
C3—N1	1.4677 (17)	N1—H11N	0.876 (15)
C6—C5	1.382 (2)	N1—H10N	0.899 (15)
O4—P1—O1	115.19 (6)	C6—C1—H1	119.7
O4—P1—O3	110.29 (6)	C3—C2—C1	118.50 (14)
O1—P1—O3	108.02 (6)	C3—C2—H2	120.7
O4—P1—O2	110.03 (7)	C1—C2—H2	120.8
O1—P1—O2	106.05 (6)	O14—C14—O13	124.25 (13)
O3—P1—O2	106.88 (7)	O14—C14—C13	121.39 (13)
P1—O2—H2O	114.7 (16)	O13—C14—C13	114.36 (13)
P1—O3—H3O	110.7 (17)	C9—C10—C11	121.68 (13)
H9B—O9—H9A	111 (2)	C9—C10—N2	119.08 (13)
O7—P2—O5	114.85 (6)	C11—C10—N2	119.24 (12)
O7—P2—O6	110.53 (7)	C8—C13—C12	119.57 (13)
O5—P2—O6	106.01 (6)	C8—C13—C14	121.60 (13)
O7—P2—O8	110.04 (6)	C12—C13—C14	118.81 (13)
O5—P2—O8	108.30 (7)	C12—C11—C10	118.71 (13)
O6—P2—O8	106.72 (7)	C12—C11—H11	120.6
P2—O6—H6O	114.2 (15)	C10—C11—H11	120.6
P2—O8—H8O	109.9 (18)	C10—C9—C8	119.12 (14)

H10B—O10—H10A	112.2 (18)	C10—C9—H9	120.4
C7—O12—H12O	109.7 (16)	C8—C9—H9	120.4
C14—O13—H13O	108.5 (17)	C9—C8—C13	120.42 (14)
C4—C3—C2	121.79 (13)	C9—C8—H8	119.8
C4—C3—N1	119.79 (13)	C13—C8—H8	119.8
C2—C3—N1	118.42 (13)	C11—C12—C13	120.49 (14)
C5—C6—C1	119.68 (13)	C11—C12—H12	119.8
C5—C6—C7	121.68 (13)	C13—C12—H12	119.8
C1—C6—C7	118.62 (13)	C10—N2—H20N	108.3 (13)
O11—C7—O12	123.99 (13)	C10—N2—H21N	108.8 (13)
O11—C7—C6	121.61 (13)	H20N—N2—H21N	112.2 (19)
O12—C7—C6	114.39 (12)	C10—N2—H22N	110.3 (12)
C6—C5—C4	120.04 (14)	H20N—N2—H22N	109.4 (18)
C6—C5—H5	120.0	H21N—N2—H22N	107.8 (17)
C4—C5—H5	120.0	C3—N1—H12N	106.9 (13)
C3—C4—C5	119.28 (13)	C3—N1—H11N	108.2 (14)
C3—C4—H4	120.4	H12N—N1—H11N	115.9 (19)
C5—C4—H4	120.4	C3—N1—H10N	110.6 (13)
C2—C1—C6	120.67 (14)	H12N—N1—H10N	109.7 (19)
C2—C1—H1	119.7	H11N—N1—H10N	105.6 (19)

2.4. Computational details

Hirshfeld surfaces computation analysis and the associated 2D fingerprint plots [22] were carried out using the Crystal Explorer 3.1 software [23] and TONTO calculation basis [24]. The surfaces were shown transparent to allow clear viewing of molecules and the crystals interaction environment. The fingerprint plots were displayed in the standard 0.4 - 3.0 Å for axes scale d_e and d_i . We used the quantities d_e and d_i to characterize the distance from Hirshfeld surface to the nearest atoms outside and inside the surface, respectively. On the d_e surfaces, the red regions indicate regions of the intermolecular contacts and in d_i surface. This indicates donor regions of intermolecular contact. The value of d_{norm} is negative or positive when intermolecular contacts are shorter or longer than van der Waals (vdw) radii of the atom enables identification of the regions of particular importance to intermolecular interactions, respectively. The d_{norm} values are mapped onto the Hirshfeld surface using a red–blue–white color codes [25–28] scheme: red regions represent closer contacts and a negative d_{norm} value; blue regions represent longer contacts and a positive d_{norm} value; and white regions represent a distance of contacts exactly equal to the vdw separation with a d_{norm} value of zero. Frontier molecular orbitals (FMOs) and electrostatic potential map were plotted using the basis set 6-311G (d,p) of the density functional theory [29]. Molecular electrostatic potential surface (MEPS) allows us to visualize variably charged regions of a molecule 29. Knowledge of the charge distributions can be used to determine how molecules interact with one another. To make the electrostatic potential energy data easy to visualize and interpret, a colour spectrum, with red as the lowest electrostatic potential energy value and blue as the highest, is employed to convey the varying intensities of the electrostatic potential energy values. They are often used for qualitative interpretation of electrophilic and nucleophilic reactions. Potential increases in the ordered < orange < yellow < green < blue.

3. Results and Discussion

3.1. Micrographs and X-ray microanalysis

The morphology of of p-Carboxyphenylammonium dihydrogenmonophosphate monohydrate crystals obtained with the scanning electron microscopy (SEM) is shown in Fig. 3. As can be seen from this figure, the compound consists of an assembly of crystal fragments having uniform distribution and a flat surface which indicates good crystal quality. The EDX (Energy dispersive X-ray) spectrum of the title compound PABADHP revealed the presence of all non-hydrogen atoms: Carbon, Nitrogen, Oxygen and phosphate. Elemental analysis of the observed atoms shows that the semi-quantitative ratios of the elements are: C: 35.1%, N: 7.6%, O: 46.5% and P: 10.9% (Fig. 4).

3.2. X-ray structure analysis

The title compound crystallizes in the triclinic system with the space group P-1 and the lattice parameters are $a=8.5304(5)$ Å, $b=8.9095(5)$ Å, $c=14.4986(8)$ Å, $\alpha=106.413(2)^\circ$, $\beta=90.158(2)^\circ$, $\gamma=92.830(3)^\circ$ with $Z=4$. The three dimensional molecular structure of the compound was determined using SHELXS and later refined by SHELXL to a final $R[F^2 > 2\sigma(F^2)]$, $wR(F^2)$, S values: 0.031, 0.093 and 1.06, respectively.

The asymmetric unit of the title compound is formed by two p-Carboxyphenylammonium, two dihydrogenmonophosphate monohydrate (Fig. 5) and two water molecules. The selected bond lengths, bond angles, and hydrogen bond data are listed in Tables 4, and 5 respectively.

In the structural arrangement (Fig. 6), the inorganic ions H_2PO_4^- , the water molecule and the organic ions $\text{C}_7\text{H}_8\text{O}_2\text{N}^+$, are interconnected through N-H \cdots O, O-H \cdots O and C-H \cdots O hydrogen bonds to form a tridimensional network (Fig. 7).

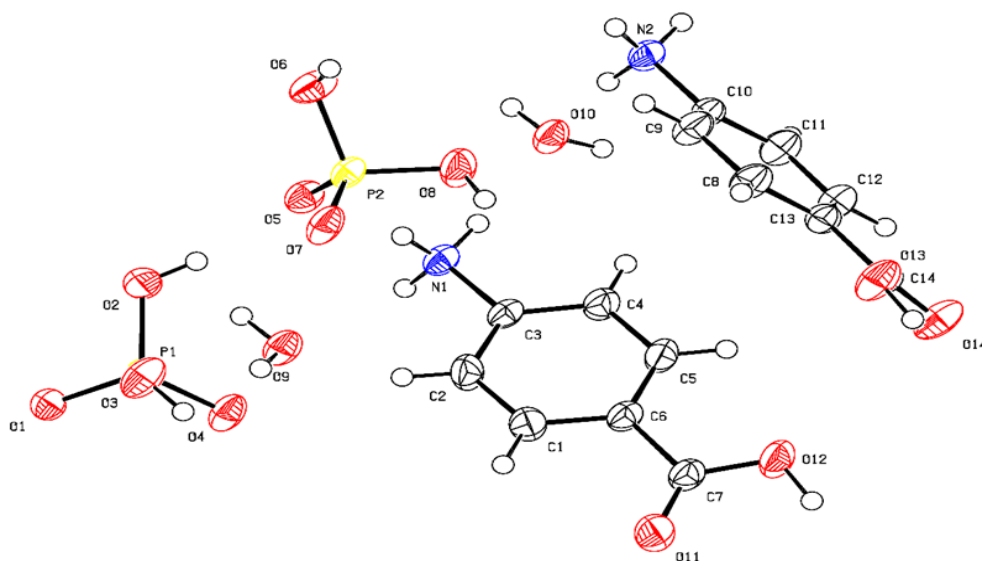


Figure 5. ORTEP of The asymmetric unit of inorganic anions, independent organic cations and water molecules of the title structure. Displacement ellipsoids are drawn at the 50% probability level.

Table 5. Hydrogen-bond geometry (Å, °).

$D-H\cdots A$	$D-H$	$H\cdots A$	$D\cdots A$	$D-H\cdots A$
C4—H4 \cdots O10	0.93	2.61	3.3105 (17)	133
C2—H2 \cdots O4	0.93	2.55	3.4664 (19)	168
C11—H11 \cdots O7 ⁱ	0.93	2.66	3.4060 (18)	138
O3—H3O \cdots O14 ⁱⁱ	0.85 (3)	1.79 (3)	2.6346 (15)	176 (3)
O6—H6O \cdots O1 ⁱⁱⁱ	0.82 (2)	1.89 (2)	2.7054 (16)	170 (2)
N1—H12N \cdots O10	0.91 (2)	1.88 (2)	2.7817 (17)	168 (2)
N1—H11N \cdots O9	0.88 (2)	2.05 (2)	2.8593 (17)	153 (2)
N1—H10N \cdots O5	0.90 (2)	1.93 (2)	2.8206 (17)	171 (2)
N2—H20N \cdots O9 ⁱⁱⁱ	0.90 (2)	1.91 (2)	2.7794 (18)	163 (2)
N2—H21N \cdots O10	0.89 (2)	1.94 (2)	2.8045 (17)	165 (2)
N2—H22N \cdots O1 ^{iv}	0.91 (1)	1.91 (2)	2.8093 (16)	171 (2)
O9—H9B \cdots O5 ^v	0.87 (2)	1.85 (2)	2.7166 (14)	171 (2)
O9—H9A \cdots O4	0.90 (2)	1.90 (2)	2.7966 (15)	174 (2)
O10—H10B \cdots O7 ⁱ	0.88 (2)	1.85 (2)	2.7263 (15)	173 (2)
O10—H10A \cdots O1 ^v	0.88 (2)	1.85 (2)	2.7176 (14)	169 (2)
O2—H2O \cdots O5	0.85 (2)	1.88 (2)	2.7238 (16)	170 (2)
O8—H8O \cdots O11 ⁱⁱ	0.83 (3)	1.81 (3)	2.6378 (15)	176 (3)

Symmetry codes: (i) $x-1, y, z$; (ii) $-x+1, -y+1, -z$; (iii) $x, y+1, z$; (iv) $x-1, y+1, z$; (v) $-x+1, -y+1, -z+1$.

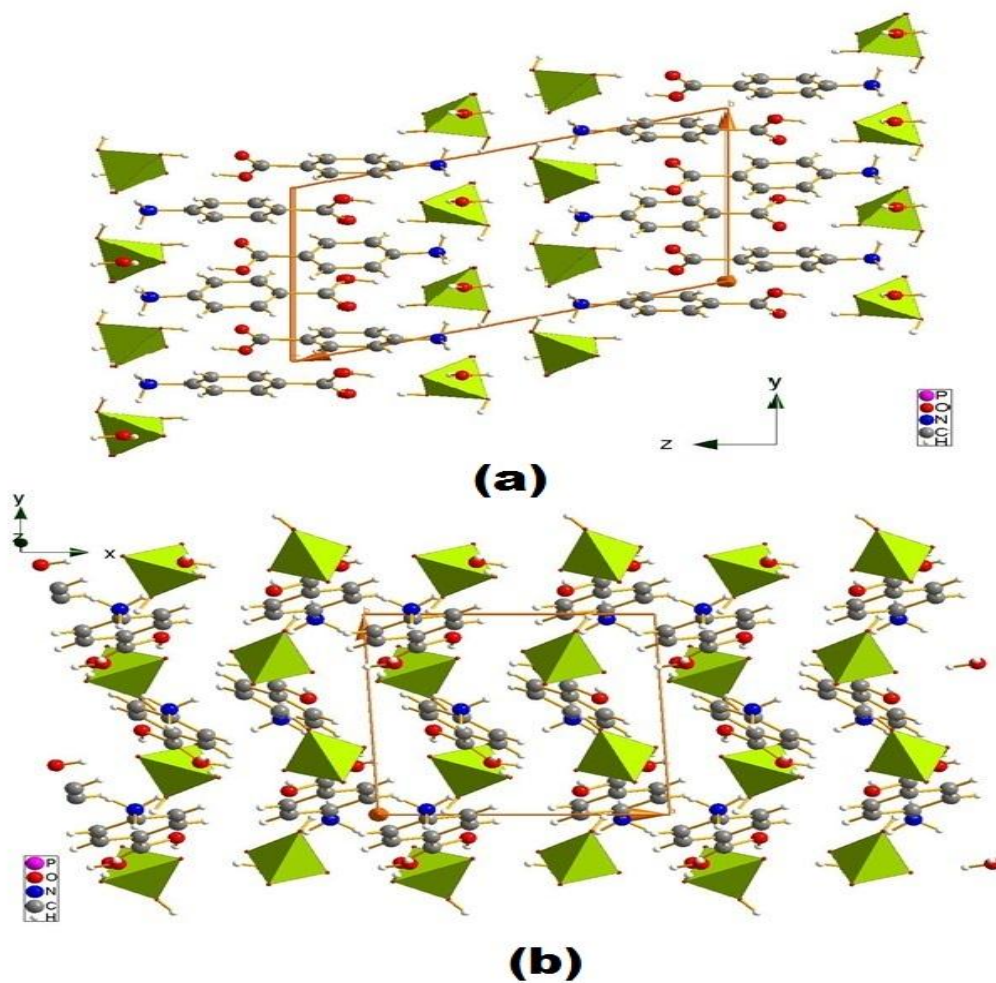


Figure 6. Projection of the structure of the PABADHP along the a axis (a) and the c axis (b).

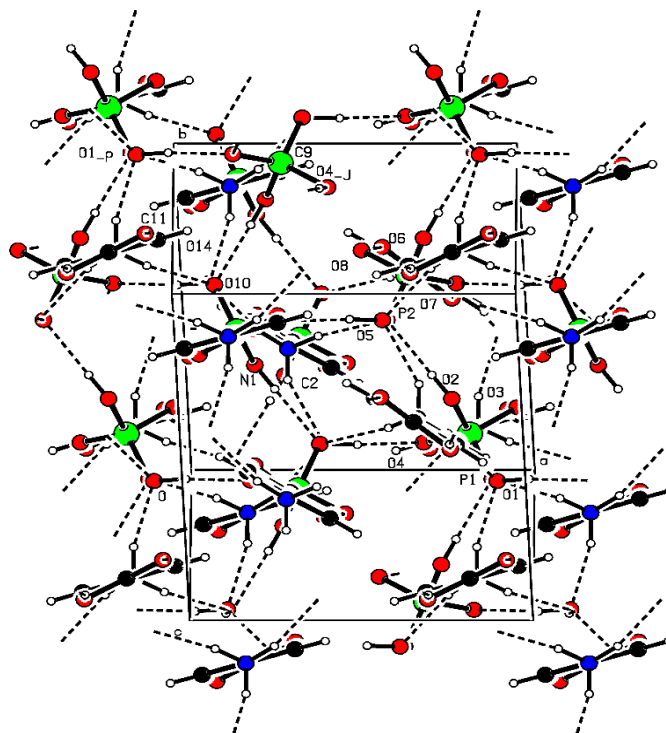


Figure 7. Hydrogen bonds in the crystal structure involving the organic part and the mineral one.

3.3. Hirshfeld surface analysis

The molecular Hirshfeld surfaces of the title compound were generated using a standard (high) surface resolution with the 3D dnorm surfaces (Fig. 8), the distance to the nearest nucleus inside the surface “ d_i ” and the distance to the nearest atoms outside “ d_e ”, shape index and curvedness mapped over a fixed color scale of -0.529 (red) to 1.263 Å (blue), from 0.609 to 2.616 Å and 0.799 to 1.352 Å, -1 to 1 Å and -4 to 0.4 Å, with:

$$d_{\text{norm}} = \frac{(d_i - r_i^{\text{vdw}})}{r_i^{\text{vdw}}} + \frac{(d_e - r_e^{\text{vdw}})}{r_e^{\text{vdw}}}$$

The 2D fingerprint maps of p-Carboxyphenylammonium dihydrogenmonophosphate monohydrate provide some quantitative information about the individual contribution of the intermolecular interaction in the asymmetric unit (Fig. 9).

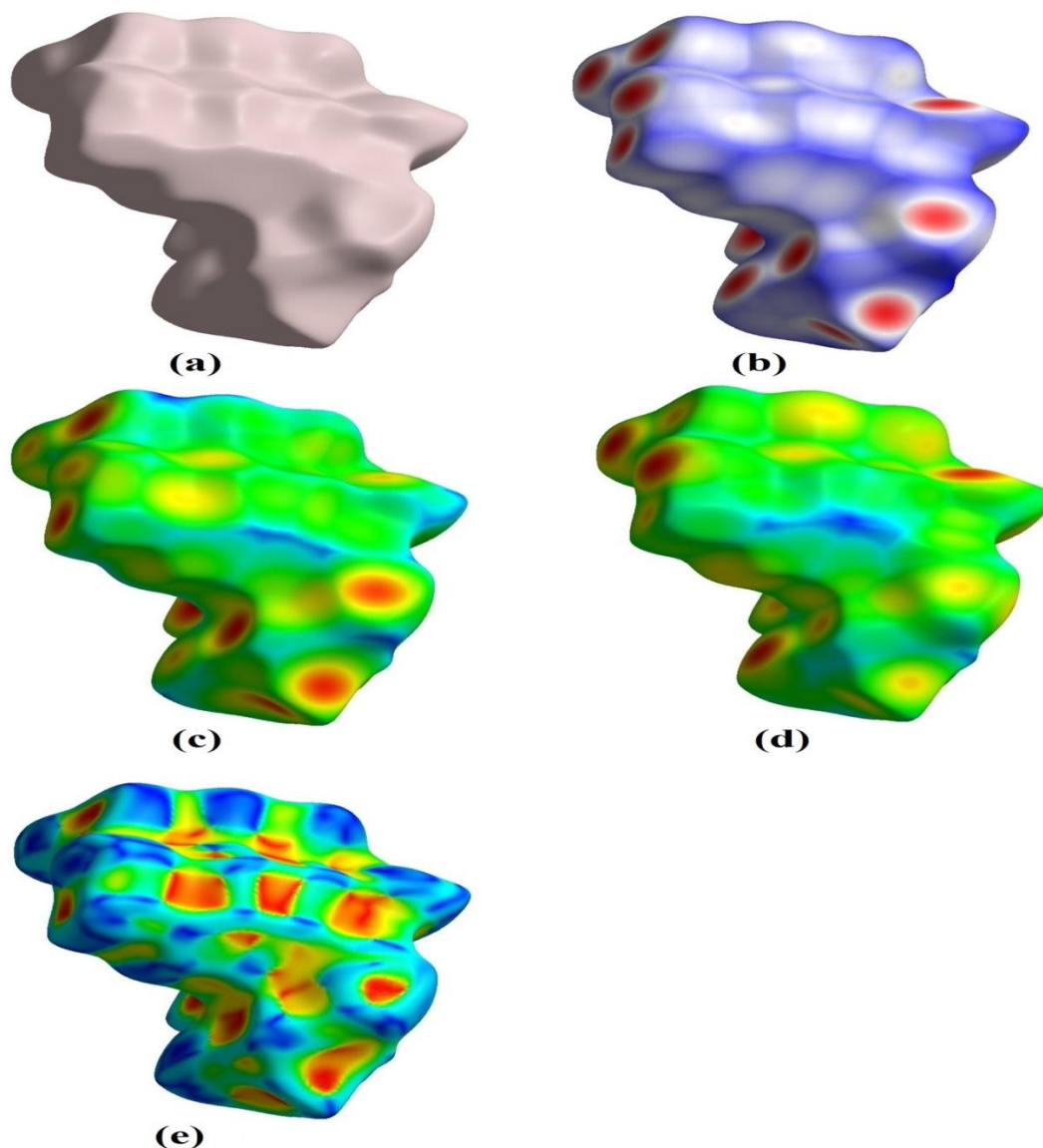


Figure 8. Hirshfeld surface analysis of PABADH:(b) dnorm, (c)de, (d)di and (e)Shape-index.

Globally, O···H/H···O and H···H intermolecular interactions were most abundant in the crystal packing (55.3% and 26.7%, respectively). It is evident that van der Waals forces exert an important influence on the stabilization of the packing in the crystal structure. Other intercontacts, i.e. C···H/H···C (8.8%), and O···C/C···O (4.1%), contribute less to the Hirshfeld surfaces. On the other hand, the Percentage contributions of the different interactions to the Hirshfeld Surfaces were also calculated for the title compound (Fig. 10).

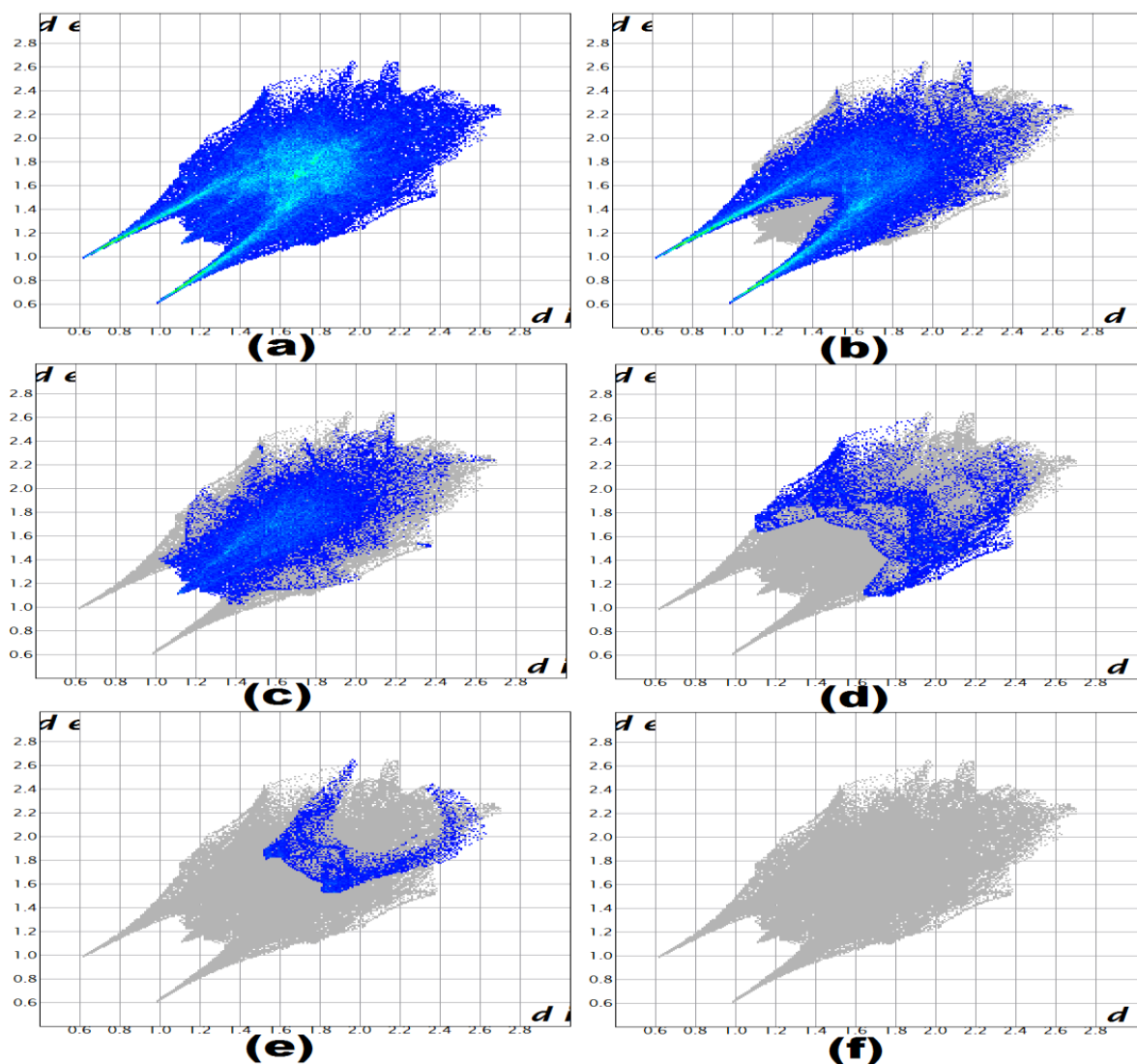


Figure 9. Fingerprint of the title compound, (b) O...H, (c) H...H, (d) C...H and (e) C...O. the different inter contacts of various intermolecular contacts contributed to the Hirshfeld surface in the compound.

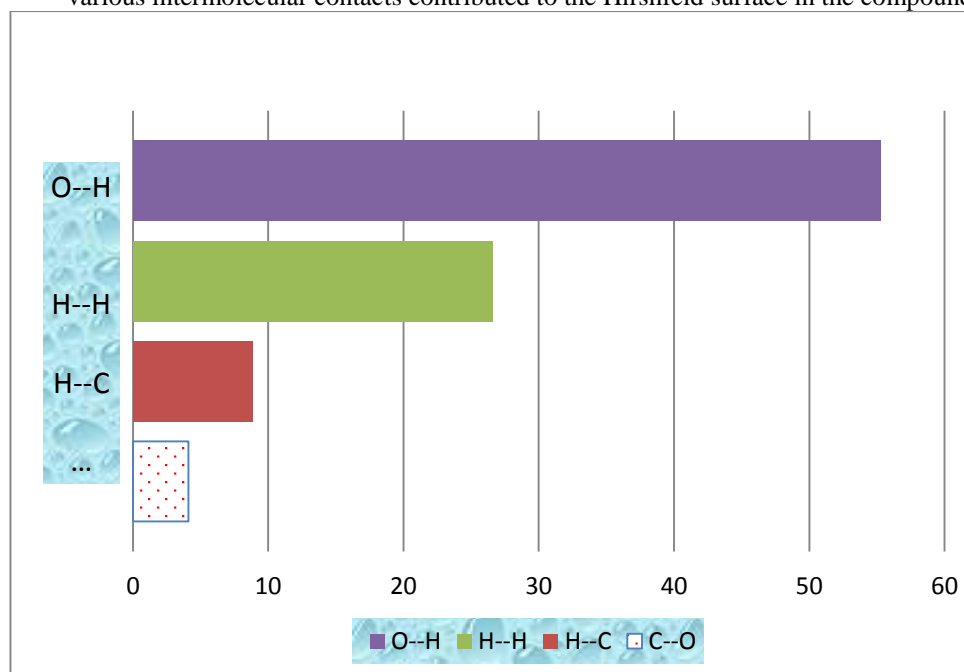


Figure 10. Percentage contribution of individual intermolecular interactions to the Hirshfeld surfaces of compound.

The electrostatic potentials were mapped on the Hirshfeld surface using the STO-3G basis set at the Hartree–Fock level of theory over the range ± 0.1 au. The contact distances d_i and d_e from the Hirshfeld surface to the nearest atom inside and outside, respectively, enables the analysis of the intermolecular interactions through the mapping of d_{norm} . The combination of d_e and d_i in the form of a two-dimensional fingerprint plot [30] provides a summary of the intermolecular contacts in the crystal. From the view of the Hirshfeld surface mapped over d_{norm} (Fig. 8), the deep-red depressions at atoms $H_{21}N$, $H_{12}N$ and O_{10} (water), $H_{10}N$ and phosphate (O_5 , O_8), $H_{11}N$ and O_9 (water) confirm their role in the N—H...O hydrogen-bond donor and acceptor, respectively. These atoms appear as the respective blue and red regions. The light-red spots near the phenylhydrogen atoms, H_4 and water-oxygen O_{10} , and H_2 atom with phosphate-oxygen O_4 , on the d_{norm} mapped surface indicate the intermolecular C—H...O interactions between them (Fig. 11).

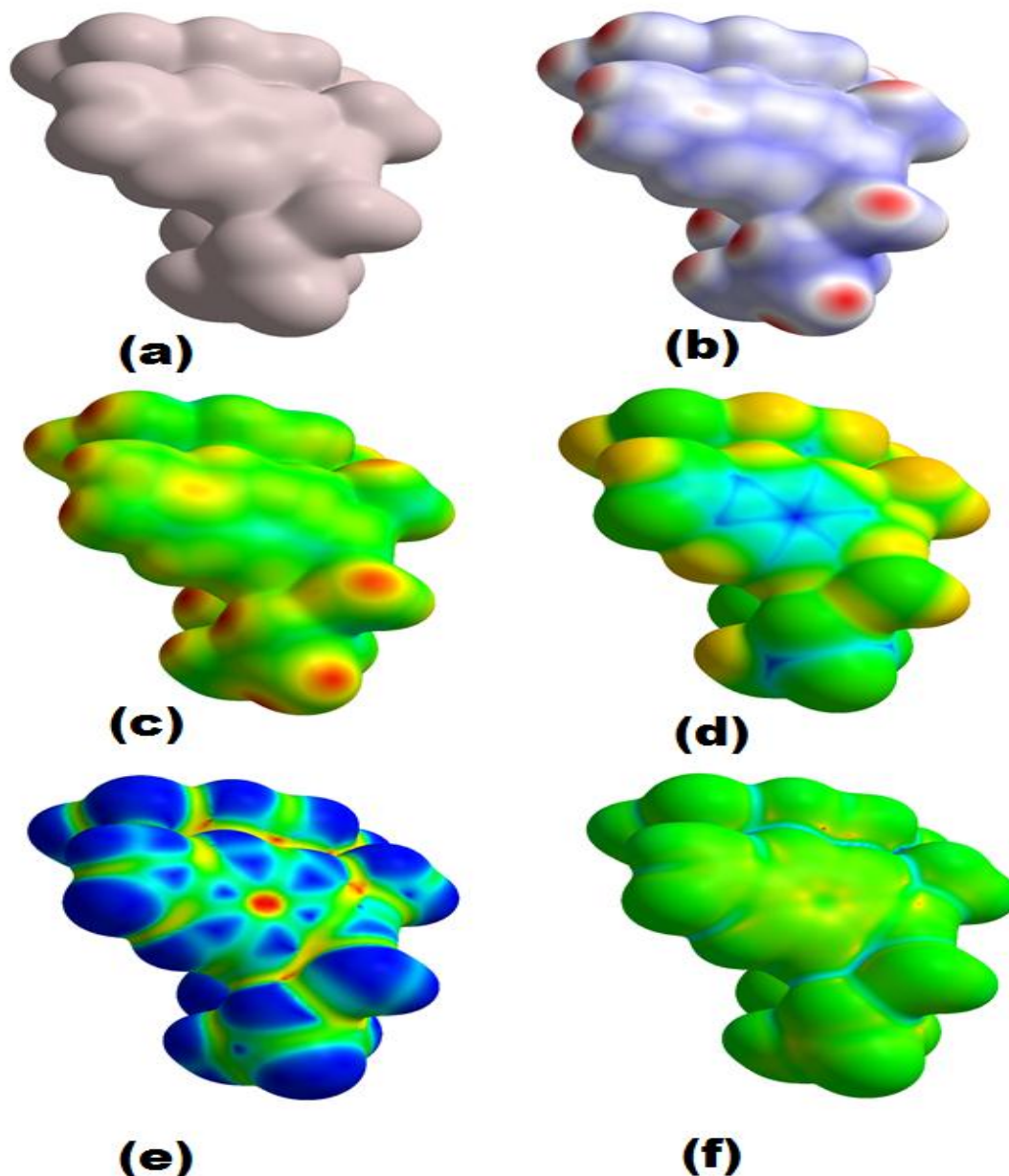


Figure 11. Electrostatic Potential (PE) mapped on Hirshfeld surface of the molecule of PABADHP: (b) d_{norm} , (c) d_e , (d) d_i , (e) Shape index and (f) Curvednes.

Fig.12. shows the voids [31] in the crystal structure of PABADHP. These are based on the sum of spherical atomic electron densities at the appropriate nuclear positions (procrystal electron density). The crystal-void calculation (results under 0.002 a.u. isovalue) shows the void volume of title compound to be of the order of $111,31 \text{ \AA}^3$ and surface area in the order of $370, 52 \text{ \AA}^2$. With the porosity, the calculated

void volume of PABADHP is 10.54%. There are no large cavities. We note that the electron-density isosurfaces are not completely closed around the components, but are open at those locations where interspecies approaches are found.

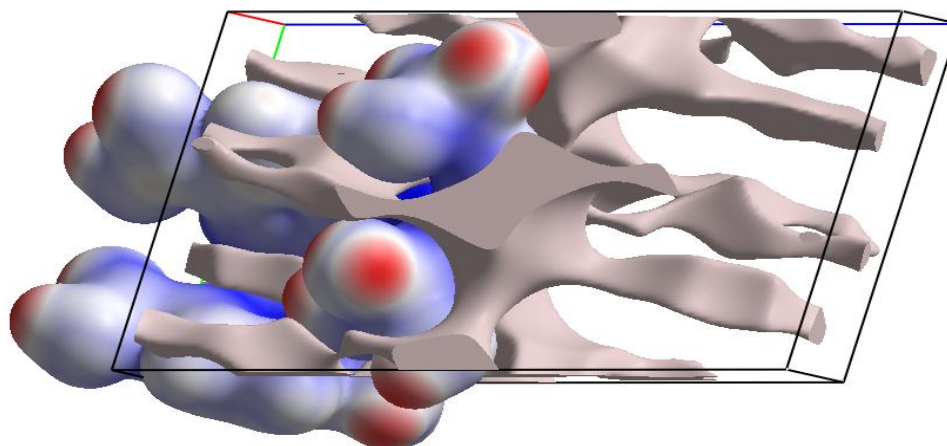


Figure 12. Crystal-void plot of the grown crystal.

4. Discussion

4.1. FT-IR spectrum analysis

In order to analyze the presence of functional groups qualitatively in a grown crystal of PABADHP, the FT-IR spectrum was recorded between 500 and 4000 cm^{-1} (Fig. 13). The resultant spectrum is shown in Table 6. The infrared spectrum exhibits the vibrations of different components of this material. Characteristic bands at 1397, 1134 and 1095 cm^{-1} are related to Stretching and symmetric stretching vibrations of P=O and P–O in plane of the phosphate groups [32], while those at 991, 951 and 882, 849 cm^{-1} are assigned to P–O–H groups. Broad bands in the range of 3220–2831 cm^{-1} correspond to O–H stretching vibrations of water molecules as well as to that of ammonium groups and in the 662 and 548 cm^{-1} clearly confirms the presence of O–P–O Bending vibrations. The observed bands in the 1657 cm^{-1} region are due to the deformation vibrations of C=C groups [33–35].

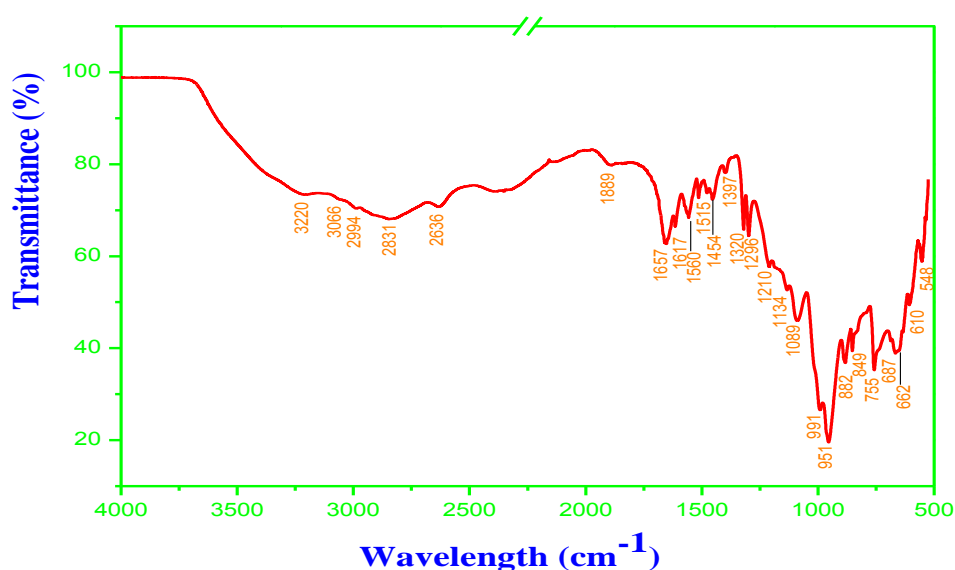


Figure13. FT-IR spectrum analysis of PABADHP compound.

Table 6. FT IR band assignments of PABADHP single crystals.

Wavelength(nm)	Tentative of assignments
3220	OH stretching
3066	NH ₃ ⁺ asymmetric stretching
2994	C-H asymmetric stretching
2831	OH stretching vibrations
2636	NH ₃ ⁺ symmetric stretching
1889	C=O stretch vibrations
1657	C=C stretching
1617	C-C stretching vibrations
1560	N-H asymmetric deformation
1515	CNH asymmetric deformation vibration
1454	C-N stretching
1397	P=O Stretching vibrations
1320	C-N Aromatic vibrations
1296	C-O stretching
1210	C-N asymmetric stretching
1134	P-O Symmetric stretching vibrations
1889	P-O ⁻ Symmetric stretching vibrations
991	P-O-H strong vibrations
951	P-O-H stretching vibrations
882	P-O-H very strong
849	P-O-H out-of-plane-bending
755	C-C skeletal stretching
662	O-P-O Bending vibrations
548	O-P-O Bending vibrations

4.2. UV-Vis spectra

The UV-Vis spectrum of the crystal is shown in Fig. 14 and shows the absorptions at 200 and 285 nm. These absorptions are attributed to π - π^* crystal transitions that are due to transitions of carboxyl group and delocalization in benzene ring [36]. The optical transmittance of the grown p-Carboxyphenylammonium dihydrogenmonophosphate monohydrate crystals, it is shown in Fig. 15.

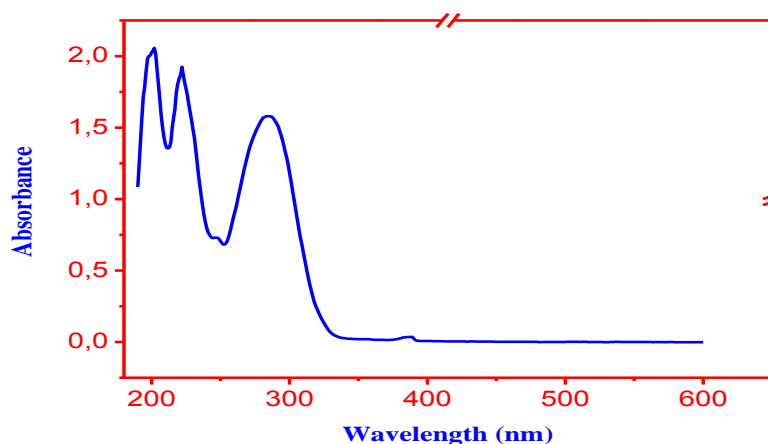


Figure14. UV-vis absorption spectrum of PABADHP crystal.

The spectrum shows a lower cut-off wavelength at 300 nm which may be due to the delocalization in the benzene ring. The transmittance between 339 and 600nm is approximately 99%. The absence of absorption in the region from 339 to 600nm indicates that the crystal suitable for optoelectronic applications. The higher intensity of absorption band presented in the UV region is due to the conjugated systems present in the grown material which may be due to π - π^* improved crystalline perfection. The good transmission optical crystals may be used for optoelectronic device applications. The absorption coefficient (α) has been calculated using the formula:

$$\alpha = \frac{2.3026 \log\left(\frac{1}{T}\right)}{t}$$

Where 'T' is the transmission and 't' is the thickness of the crystal. Optical band gap (E_g) is evaluated from the transmission spectrum and optical absorption coefficient (α) near the absorption edge and it is given by :

$$h\nu\alpha = A(h\nu - E_g)^{\frac{1}{2}}$$

Where 'A' is a constant, ' E_g ' is the optical band gap, 'h' is the Planck's constant and ' ν ' is the frequency of the incident photons. Optical band of the material was calculated by extrapolation of the linear part of the curve to apoint $(\alpha h\nu)^2$ with $h\nu$ [37]. The optical band gap was found to be equal to 3.9 eV (Fig. 16). The large transmittance in the visible region and wide band gap makes the crystal suitable for optical applications.

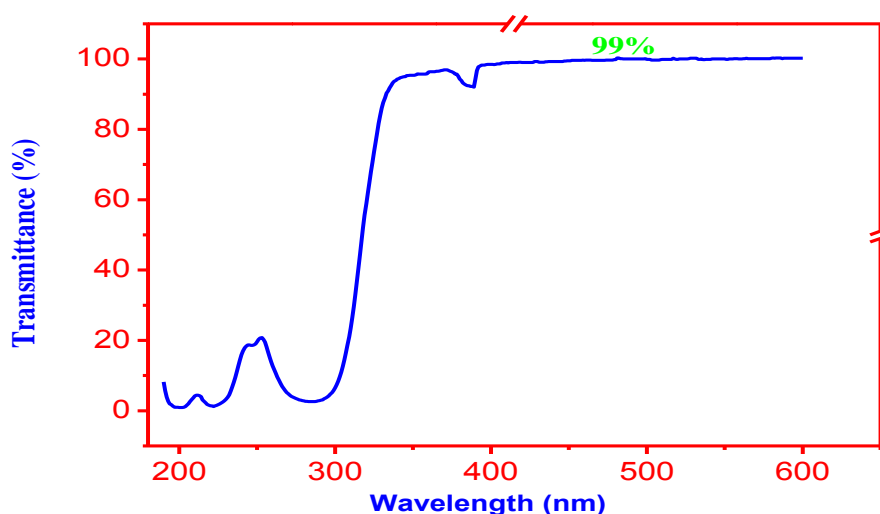


Figure 15. Optical transmittance spectrum of PABADHP crystal.

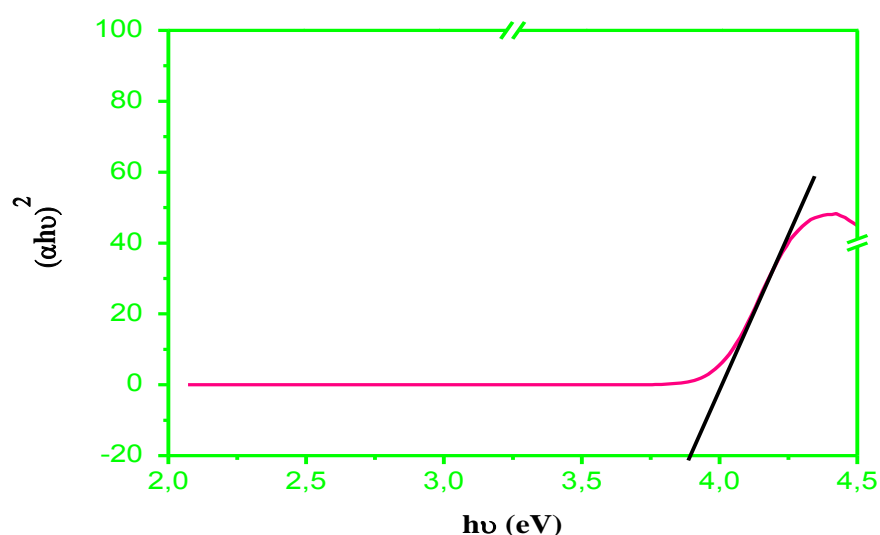


Figure16. Plot of $h\nu$ vs. $(\alpha h\nu)^2$.

4.3. Frontier molecular orbital analysis (FMO)

The frontier molecular orbitals formed by the HOMO (Highest Occupied Molecular Orbital) and the LUMO (Lowest Unoccupied Molecular Orbital) are the most popular quantum mechanical descriptors which define the reactivity of the studied compound. The energy of the HOMO is, essentially, related to

the ionization potential. Also, it is useful to discuss the electrophilic behavior of the studied hybrid. Accordingly, the energy of LUMO is basically related to the nucleophilic activities of the compound. The map of frontier molecular orbitals of the title molecule is illustrated in Fig. 17. The HOMO and LUMO of the title compound are localized over part of oxygen atoms of H_2PO_4^- anion and part of protonated p-Carboxyphenylammonium. We can calculate the energy gap ($E_g = E_{\text{LUMO}} - E_{\text{HOMO}}$) of the title compound, as $E = 3.7 \text{ eV}$ for HOMO \rightarrow LUMO.

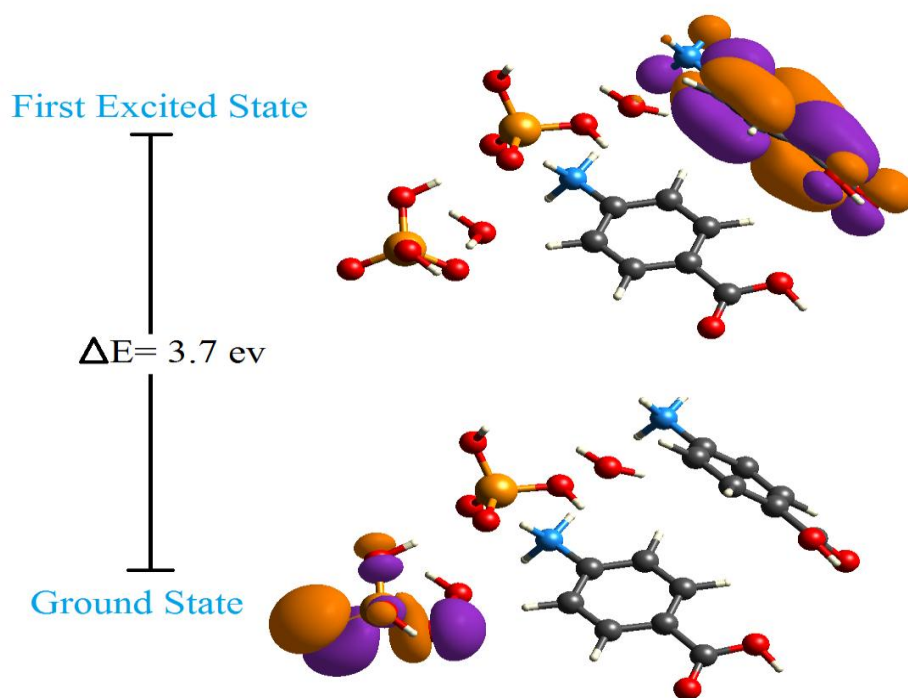


Figure17. Frontier molecular orbital plots of PABADHP.

Conclusion

Synthesis, growth and characterization of a new hybrid, p-Carboxyphenylammonium di hydrogenmonophosphate monohydrate, is presented. The Single crystal XRD analysis established the supramolecular nature of the crystal structure. The molecular structure was further probed by modern spectroscopic techniques. The presence of phosphate moiety in PABADHP is unambiguously confirmed from EDAX spectrum. The transparency of PABADHP crystal in the visible region reveals its suitability for optical application. The strong hydrogen bonding interactions between p-Carboxyphenylammonium and phosphate molecules is established by the molecule of water.

The 3D Hirshfeld surface analysis with 2D fingerprint plots reveals the percentages of the intermolecular contacts of the title compound. It has been stated that the N...O interactions have the most important percentage of the total surface, and this indicates the existence of appreciable hydrogen bonding. The importance of phosphate anion in the PABADHP crystal structure for the enhancement of nonlinear optical activities is also illustrated.

Acknowledgements-The author is thankful to the University Ibn Tofail, Kénitra, Morocco, for financial support, and CAC- Cadi Ayyad University for the help with MEB-EDAX.

References

1. J. Kroupa, A. Fuith, ptical study of the successive phase transitions of n-alkyl ammonium dihydrogen phosphate crystals, *Phys. Rev. B*, 48, (1993) 4119–4121. <https://doi.org/10.1103/PhysRevB.48.4119>

2. M.I. Khan, R.C. Nome, S. Deb, J.H. McNeely, B. Cage, R.J. Doedens, Inorganic–Organic Hybrid Materials with Novel Framework Structures: Synthesis, Structure, and Magnetic Properties of $[\text{Ni}(\text{py})_4]_2\text{V}_{10}\text{O}_{29}$ and $[\text{Ni}_2(\text{py})_5(\text{H}_2\text{O})_3]\text{V}_4\text{O}_{12}$, *Cryst. Growth Des.*, 9 (2009) 2848–2852. <https://doi.org/10.1021/cg9001237>
3. I.R. Evans, J.A.K. Howard, J.S.O. Evans, Structural ferroelectric phase transition and polymorphism in 2-aminopyridine dihydrogen phosphate, *Cryst. Growth Des.*, 8 (2008) 1635–1639. <https://doi.org/10.1021/cg701076s>
4. P. Balamurugan, R. Jagan, K. Sivakumar, Dihydrogen phosphate mediated supramolecular frameworks in 2- and 4-chloroanilinium dihydrogen phosphate salts, *Acta Cryst.* C66 (2010) o109–o113. <https://doi.org/10.1107/S0108270110001940>
5. K. H. Dipak, C. Rajarshi, A. Mahammad, M. Monika, 4-(3,5-Dimethyl-1H-pyrazol-4-ylmethyl)-3,5-dimethyl-1H-pyrazol-2-ium dihydrogen phosphate: a combined X-ray and DFT study, *Acta Cryst.* C66 (2010) o190–o193. <https://doi.org/10.1107/S0108270110007134>
6. K. Russel Raj, P. Murugakoothan, Studies on the optical and mechanical properties of non-linear optical 3-aminophenol orthophosphoric acid (3-amphph) single crystal, *J. Optik.*, 123 (2012) 1082–1086. <https://doi.org/10.1016/j.ijleo.2011.07.036>
7. P. Nagapandiselvi, C. Baby, R. Gopalakrishnan, Synthesis, growth, structure and nonlinear optical properties of a semiorganic 2-carboxy pyridinium dihydrogen phosphate single crystal, *J. Optical Materials*, 47 (2015) 398–405. <http://doi.org/10.1016/j.optmat.2015.06.012>
8. T. Ben Issa, H. Ghalla, S. Marzougui, L. Benhamada, Crystal structure and theoretical studies on quinoline phosphate, *J. molstruc.*, 1150 (2017) 127–134. <https://doi.org/10.1016/j.molstruc.2017.08.086>
9. A. Ben Ahmed, H. Feki, Y. Abid, H. Boughzala, C. Minot, A. Mlayah, Crystal structure, vibrational spectra and theoretical studies of L-histidinium dihydrogen phosphate-phosphoric acid, *J. Mol. Struc.*, 920 (2009) 1–7. <https://doi.org/10.1016/j.molstruc.2008.09.029>
10. S.Z. Siddiqui, U. Waqas, M. Akkurt, R. Aziz-ur, I.U. Khan, 2-Amino-1,3-benzothiazol-3-iumdihydrogen phosphate, *J. Acta Cryst.* E66 (2010) o1929. <https://doi.org/10.1107/S1600536810025547>
11. PAR A. CARPY, M. GADRET, J.M. LEGER, Phosphate de Xylazine: Phosphate de N-(Diméthyl-2,6 ph6nyl-dihydro-5,6 4H-Thiazine- 1,3 Amine-2, *J. Acta Cryst.* B35 (1979) 994–996. <https://doi.org/10.1107/S0567740879005380>
12. D. Amel, S.S. Leila, D. Ahmed, A new amine phosphate template bytris(2-aminoethyl)amine, *J. Acta Cryst.* E60 (2004) o2241–o2243. <https://doi.org/10.1107/S1600536804027540>
13. C. Muthuselvi, N. Mala, N. Srinivasan, S. Pandiarajan, R.V. Krishnakumar, Crystal structure of 4-sulfamoylaniliniumdihydrogen phosphate, *J. Acta Cryst.* E70 (2014) o997–o998. <https://doi.org/10.1107/S1600536814017462>
14. O. Kaman, L. Smrcok, R. Gyepes and D. Havlíček, Anilinium dihydrogen phosphate, *J. Acta Cryst.* C68 (2012) o57–o60. <https://doi.org/10.1107/S0108270111054874>
15. V. Langer, K. Huml, J. Zachová, The crystal and molecular structure of adeninium phosphate, $\text{C}_5\text{H}_6\text{N}_5^+ \cdot \text{H}_2\text{PO}_4^-$, *J. Acta Cryst.* B35 (1979) 1148–1152. <https://doi.org/10.1107/S0567740879005768>
16. S. Shylaja, K.N. Mahendra, K.B.R. Varma, T. Narasimhamurthy, R.S. Rathore, Hydrogen-bonded sheets in 2-(2-aminophenyl)-1H-benzimidazol-3-ium dihydrogen phosphate, *J. Acta Cryst.* C64 (2008) o361–o363. <https://doi.org/10.1107/S010827010801456X>
17. S. Thangarasu, S.S. Kumar, S. Athimoolam, B. Sridhar, S.A. Bahadur, R. Shanmugam, A.T. Chelvam, Synthesis, structure, spectral, thermal analyses and DFT calculation of a hydrogen bonded crystal: 2-aminopyrimidinium dihydrogen phosphate monohydrate, *J. Mol. Struc.*, 1074 (2014) 107–117. <https://doi.org/10.1016/j.molstruc.2014.05.054>
18. G.M. Sheldrick, SHELXS97 and SHELXL97. Program for Crystal Structure Solution and Refinement. University of Göttingen, Göttingen, (1997).
19. G.M. Sheldrick, A short history of SHELX. *Acta Cryst.* A64 (2008) 112–122. <https://doi.org/10.1107/S0108767307043930>
20. A.L. Spek, Determination of the stress orientation distribution function using pulsed neutron sources, *J. Appl. Cryst.* 36 (2003) 7–13. <https://doi.org/10.1107/S0021889802017399>
21. K. Brandenburg, H. Putz DIAMOND Version3. Crystal Impact GbR, Postfach (2005) 1251, D-53002 Bonn, Germany.
22. M.A. Spackman, J.J. McKinnon, Fingerprinting intermolecular interactions in molecular crystals, *CrystEngComm*, 4 (2002) 378–392. <https://doi.org/10.1039/B203191B>

23. S.K. Wolff, D.J. Grimwood, J.J. McKinnon, M.J. Turner, D.a. Jayatilaka, M.A. Spackman CRYSTALEXPLORER 3.0 University of Western Australia, Perth (2012).
24. D. Jayatilaka, D.J. Grimwood and Lee A TONTO A System for Computational Chemistry (Nedlands: The University of Western Australia) (2005).
[http://crystalexplorer.scb.uwa.edu.au/wiki/index.php/TONTO: A System For Computational Chemistry](http://crystalexplorer.scb.uwa.edu.au/wiki/index.php/TONTO:_A_System_For_Computational_Chemistry)
25. Y.H. Luo, Q.X. Mao, B.W. Sun, Two new complexes with 6-methylnicotinic acid ligand: Synthesis, crystal structure and Hirshfeld surfaces, *Inorg. Chim. Acta*, 412 (2014) 60. <https://doi.org/10.1016/j.ica.2013.12.005>
26. Y.H. Luo, B.W. Sun, Pharmaceutical co-crystals of pyrazinecarboxamide (PZA) with various carboxylic acids: crystallography, Hirshfeld surfaces, and dissolution study, *Cryst. Growth Des*, 13(2013) 2098. <https://doi.org/10.1021/cg400167w>
27. Y.H. Luo, B. Xu, B.W. Sun, Investigation of supramolecular synthons of p-hydroxybenzoic acid (PHBA): Comparison of its hydrate, co-crystal and salt, *J. Cryst. Growth*, 374 (2013) 88. . <https://doi.org/10.1016/j.jcrysgro.2013.03.007>
28. G.R. Desiraju, A. Gavezzotti Crystal structures of polynuclear aromatic hydrocarbons Classification, rationalization and prediction from molecular structure, *Acta Crystallogr. Sec. B*, 45(1989) 473. <https://doi.org/10.1107/S0108768189003794>
29. A. Becke, Density-Functional Thermochemistry. III. The Role of Exact Exchange, *J. Chem. Phys*, 98 (1993)5648–5652. <https://doi.org/10.1063/1.464304>
30. A.L. Rohl, M. Moret, W. Kaminsky, K. Claborn, J.J. McKinnon, B. Kahr, Hirshfeld Surfaces Identify Inadequacies in Computation of Intermolecular Interactions in Crystals: Pentamorphic 1,8-Dihydroxyanthraquinone, *Cryst. Growth Des*, 8 (2008)4517–4525. <https://doi.org/10.1021/cg8005212>
31. T. Nidhi, S. Nidhi, Y. Harsh, K. Binay, Enhancement of Optical, Piezoelectric, and Mechanical Properties in Crystal Violet Dye-Doped Benzophenone Crystals Grown by Czochralski Technique, *Cryst. Growth Des*, 10 (2015) 4908-4917. <https://doi.org/10.1021/acs.cgd.5b00792>
32. K. Rajendran, C. Dale keefe, Growth and characterization of calcium hydrogen phosphate dihydrate crystals from single diffusion gel technique, *Cryst. Res. Technol*, 45 (2010) 939–945. <https://doi.org/10.1002/crat.200900700>
33. V. Koleva, V. Stefov, A. Cahil, M. Najdoski, B. Šoptrajanov, B. Engelen, H.D. Lutz, Infrared and Raman studies of manganese dihydrogen phosphate dihydrate, $Mn(H_2PO_4)_2 \cdot 2H_2O$. I: Region of the vibrations of the phosphate ions and external modes of the water molecules, *J. Mol. Struct.* 917 (2009) 117. <https://doi.org/10.1016/j.molstruc.2008.07.002>
34. B. Abir, J. S. Jean, B. Mohamed, Crystal structure, vibrational studies and optical properties of a new organic phosphate $(C_{12}H_{14}N_2S)(H_2PO_4)_2$, *J. Mol. Struct*, 120 (1995) 343. <https://doi.org/10.1016/j.molstruc.2018.06.115>
35. D.V. Giancarlo, C. Francesco, C. Giancarlo, V. Gennaro, M. Alessandro, X-ray Structure Refinement and Vibrational Spectroscopy of Metavauxite $FeAl_2(PO_4)_2(OH)_2 \cdot 8H_2O$, *J. Crystals*, 9 (2019) 297. <https://doi.org/10.3390/cryst9060297>
36. K.C. Senthil, P. Rajesh, P. Ramasamy, Structural, optical, thermal, photoconductivity, laser damage threshold and fluorescence analysis of an organic material: β -P-amino benzoic acid single, *J. Optical Materials*, 52 (2016) 49–55. <https://doi.org/10.1016/j.optmat.2015.11.044>
37. J. Tauc, Amorphous and Liquid Semiconductors, *Plenum*, New York, (1974).

(2020) ; <http://www.jmaterenvirosci.com>